Materials Today Physics 46 (2024) 101500

Contents lists available at ScienceDirect

Materials Today Physics

journal homepage: www.journals.elsevier.com/materials-today-physics

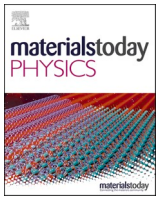

Isotope interface engineering for thermal transport suppression in cryogenic graphene

Xin Wu [a,b,*], Yunhui Wu [a], Xin Huang [a], Zheyong Fan [c], Sebastian Volz [a,d], Qiang Han [b,**], Masahiro Nomura [a,***]

[a] Institute of Industrial Science, The University of Tokyo, Tokyo, 153-8505, Japan
[b] Department of Engineering Mechanics, School of Civil Engineering and Transportation, South China University of Technology, Guangzhou, Guangdong Province, 510640, China
[c] College of Physical Science and Technology, Bohai University, Jinzhou, 121013, China
[d] Laboratory for Integrated Micro and Mechatronic Systems, CNRS-IIS UMI 2820, The University of Tokyo, Tokyo, 153-8505, Japan

ARTICLE INFO

Keywords:
Cryogenic thermal properties
Graphene
Isotope interface
Golomb ruler

ABSTRACT

The development of emerging technologies, such as quantum computing and semiconductor electronics, emphasizes the growing significance of thermal management at cryogenic temperatures. Herein, by designing isotope interfaces based on the Golomb ruler, we achieved effective suppression of the phonon thermal transport of cryogenic graphene. The pronounced disordering of the Golomb ruler sequence results in the stronger suppression of thermal transport compared to other sequences with the same isotope doping ratio. We demonstrated that the Golomb ruler-based isotope interfaces have strong scattering and confinement effects on phonon transport via extensive molecular dynamics simulations combined with wave packet analysis, with a proper correction for the missing quantum statistics. This work provides a new stream for the design of thermal transport suppression under cryogenic conditions and is expected to expand to other fields.

1. Introduction

Driven by strong impetus, the need for thermal management at cryogenic temperatures is rapidly emerging in several fields [1,2] including quantum computing, quantum communication, life sciences, etc. The accuracy and long-term stability of qubits, information units in quantum computers, necessitate an environment of cryogenic temperatures to ensure their reliability [1]. In the field of life sciences, cryopreservation technology at cryogenic temperatures holds great significance for safeguarding biological diversity and advancing the frontiers of genetic medicine [3]. Moreover, running semiconductor electronics specifically designed for and operated at cryogenic temperatures is expected to produce more efficient systems compared to room temperature (RT) operation, which benefits from better electronics and thermal properties [4,2]. Due to many-body interactions and thermal excitations, many quantum effects cannot be observed in the macroscopic world. However, as the temperature gradually decreases, those quantum and condensation phenomena masked by thermal excitations will emerge bit by bit. For instance, when the temperature is slightly lower than 4.2 K, the electric resistance of mercury suddenly disappears, showing superconductivity [5]. Therefore, exploring cryogenic thermophysics promises to achieve more effective and reliable thermal management.

Following the successful preparation of graphene, a large number of two-dimensional (2D) materials have been developed one after another, demonstrating sustained high-level innovation vitality [6–8]. The vast available data and high-performance device demonstrations are indicative of the potential of 2D materials for applications in electronics [9,10], thermoelectronics [11–14], and sensing [15,16]. They have attracted a lot of attention from the scientific community and industry in the field of thermal management, from basic theoretical research to applications. This includes, but is not limited to, research on phonon hydrodynamic transport phenomena [17–19], modulation of thermal properties by interface and strain engineering [20,21], exploration of thermal functionality, for example, rectification effects [22]. Reducing the thermal conductivity of materials has long been a topic of

* Corresponding author. Institute of Industrial Science, The University of Tokyo, Tokyo, 153-8505, Japan.
** Corresponding author.
*** Corresponding author.
E-mail addresses: xinwu@iis.u-tokyo.ac.jp (X. Wu), emqhan@scut.edu.cn (Q. Han), nomura@iis.u-tokyo.ac.jp (M. Nomura).

https://doi.org/10.1016/j.mtphys.2024.101500
Received 1 May 2024; Received in revised form 22 June 2024; Accepted 8 July 2024
Available online 11 July 2024

widespread attention and discussion [12,23,24], and this holds true even under cryogenic temperatures. It plays a pivotal role in sustaining low-temperature states within cryogenic equipment and superconducting applications, thereby augmenting their performance and stability.

It should be noted that experimental measurement of the thermophysical properties of independently suspended 2D materials has always been a thorny topic. Fortunately, first-principles calculations and molecular dynamics (MD) simulations provide good solutions for predicting the physical properties of materials [25]. However, the former is limited by high computational costs and is difficult to evaluate for large-scale systems. Due to the statistical overestimation of the heat capacity of solids at cryogenic temperatures where quantum effects are significant [26,27], general MD simulations are also limited to the medium-to-high temperature range. Previous researches tend to focus on room temperature and above, which is the temperature range of interest for traditional electronic devices. Understanding the modulation of thermal transport properties in 2D materials at cryogenic temperatures remains relatively unexplored.

In this work, inspired by the Golomb ruler sequence, graphene nanoribbons containing linear isotope interfaces were constructed and efficient suppression of phonon thermal transport was achieved at a cryogenic temperature of 20 K. Compared with other sequences such as Equidistant and Fibonacci, the extremely strong disordering of the Golomb ruler sequence makes the isotope interfaces have a stronger scattering and confinement effect on the phonon transport. The isotope interfaces arranged according to the Golomb ruler sequence greatly impede the phonon transport over a wide spectral range. Through phonon analysis of a pair of systems, based on a Golomb ruler and an equidistant structure, the results indicated that the difference in the phonon mean free path (MFP) of low-frequency out-of-plane phonons is a crucial factor for the difference in thermal conductivity. This effect is notably pronounced at cryogenic temperatures where phonon energies are lower, otherwise, higher phonon energies render phonon transport less sensitive to differences in isotopic interface positions. Furthermore, the isotope interface density and doping ratio have no significant impact on thermal conductivity at cryogenic temperatures. Hence, this study provides valuable insights into cryogenic thermal management and is expected to inspire extensive theoretical research and practical micro-nano applications.

2. Model and methods

In mathematics, a Golomb ruler is defined as a collection of marks positioned at integer locations along a ruler, ensuring that no two pairs of marks share identical distances [28,29]. The number of marks on the ruler is its order, and the largest distance between two marks is its length. The schematic diagram of the 9th-order Golomb ruler with a length of 44 is shown in Fig. 1, in which the circular display mode is used to save space. On the basis of this configuration, treating the graphene nanoribbon as a ruler and building the interfaces at Golomb ruler marks can obtain the interface-containing graphene based on Golomb ruler sequences.

In graphene, isotope doping is usually regarded as an effective means of thermal performance modulation, which is effective in enhancing local phonon scattering and reducing system harmonicity [30,31,32]. In contrast to grain boundary phonon scattering [33], which results from direct phonon scattering caused by discontinuities in the lattice structure, isotope scattering is caused by changes in local lattice vibration modes due to the difference in isotope mass. Generally speaking, the latter has less influence on the phonon free path and can be artificially adjusted through distribution and concentration of isotopes [34]. There are two stable isotopes for carbon: ^{12}C and ^{13}C, with a natural abundance of 98.9 % and 1.06 % respectively [35]. We designed a graphene model with ^{13}C isotope linear interfaces based on the 9th-order Golomb ruler sequence (Fig. 1(b) upper). For one thing, previous research has verified that the higher-order Golomb ruler sequence has a more significant suppression effect on thermal transport [36]; for another, unlike other orders, there is only one case for an optimal sequence of the ninth order, and the computational cost is not particularly high. In terms of comprehensive effectiveness and cost, we selected the ninth-order Golomb ruler as the only research object in the current study.

For comparison purposes, a graphene model with equidistant interfaces (Fig. 1(b) bottom) was also constructed. The only distinction between them lies in the distances between the interfaces. They constitute a pair of ideal systems for studying the effect of interface locations on phonon thermal transport. Here are two adjustable structural variables: the interface density and the isotope doping ratio. We define

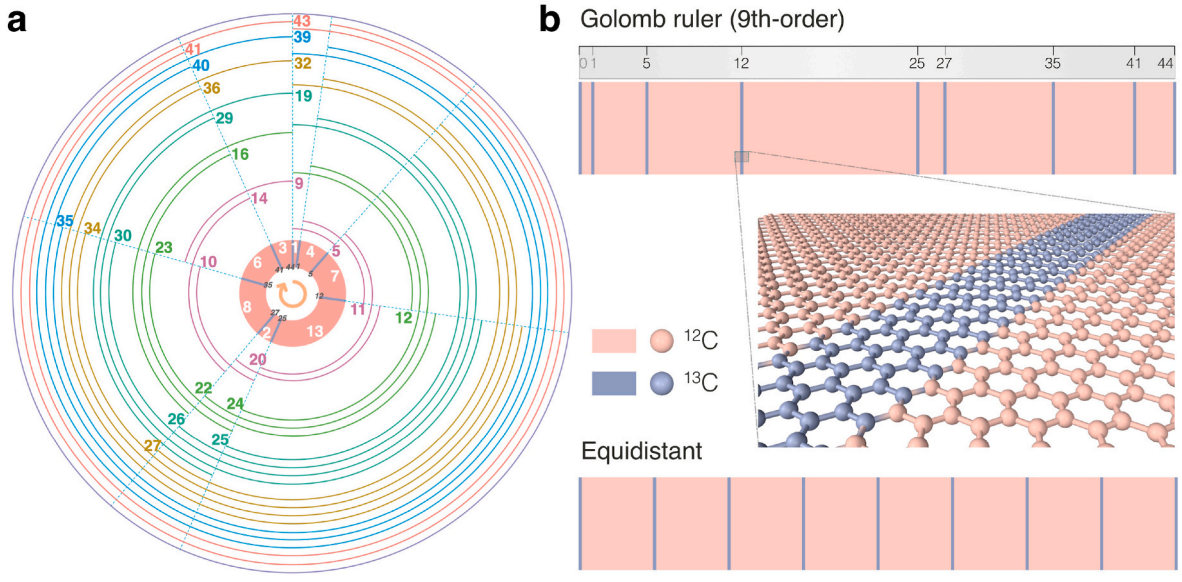

Fig. 1. Schematic diagram of graphene with isotope interfaces. (a) The optimal circular Golomb ruler of the ninth order. The red annulus in the center is obtained by curling the Golomb ruler to occupy less display space, and the blue spacer bars in it are the scales of the Golomb ruler. The numbers in different colors represent the spacing between every 2 bars, which are all different. (b) Schematic diagram of isotope interface graphene optimized by the ninth order Golomb ruler, and the equidistant one with the same interface density.

the unit length in the Golomb ruler as the basic unit of structural length, and its physical length is an integer multiple of the lattice length of a complete hexagonal ring. Furthermore, by adjusting this multiple, models with different interface densities can be obtained, where the interface density is defined as number of interfaces per unit length and calculated by the ratio of the number of interfaces to the length of the model. The latter is quantified mainly by controlling the number of ^{13}C–^{13}C bonds at the interface. The isotope doping ratio is specifically defined as the ratio of the total number of ^{13}C atoms to the total number of atoms in the system. We used homogeneous non-equilibrium molecular dynamics (HNEMD) [37,38], non-equilibrium molecular dynamics (NEMD) [39] and related spectral decomposition methods [38,40,41] as implemented in graphics processing units molecular dynamics (GPUMD) [42].

Specifically, HNEMD method simulates the effect of thermal gradients by applying a suitable virtual force field to the system along a fixed direction and achieves the calculation of thermal conductivity through the linear response of the virial heat flux vector with respect to the heat flow vector. Combining it with the Green-Kubo relation [43,44] gives the following results for the running thermal conductivity:

$$\kappa(t) = \frac{1}{k_B T^2 V}\int_0^t \langle \vec{Q}(t')\vec{Q}(0)\rangle dt' = \frac{\langle \vec{Q}(t)\rangle_{ne}}{TVF_e} \quad (1)$$

The F_e denotes the modulus of the driving force vector, the measure of which is the reciprocal of the length. It is fundamental for the system to achieve a perfectly linear response with a sufficiently large signal-to-noise ratio to give satisfactory results. Moreover, by incorporating the virial velocity correlation function within a non-equilibrium steady state framework, it becomes possible to perform the spectral decomposition of heat current, thereby facilitating the spectral decomposition of thermal conductivity $\kappa(\omega)$ (HNEMD) and thermal conductance $G(\omega)$ (NEMD). The former corresponds to the transport coefficients for infinite systems, while the latter targets the quasi-ballistic transport phase for finite systems. The combination of the two and extrapolation enables the prediction of length-dependent thermal conductivity results.

Further, the effect of possible phonon localization effects on thermal transport is also considered by calculating phonon participation rates (PPR). Without the lattice dynamics calculations, the PPR can be calculated directly by phonon density of states (PDOS) results from MD simulations, which can implicitly include anharmonic scattering of all orders:

$$\mathrm{PPR}(\omega) = \frac{1}{N}\frac{\left(\sum_i \mathrm{PDOS}_i^2(\omega)\right)^2}{\sum_i \mathrm{PDOS}_i^4(\omega)} \quad (2)$$

where N is the total number of atoms involved in the calculation, and PDOS can be obtained based on the velocity auto-correlation function of the atoms in different directions:

$$\mathrm{PDOS}_{i\alpha}(\omega) = \int_{-\infty}^{+\infty} \langle v_{i\alpha}(t)v_{i\alpha}(0)\rangle e^{-2\pi i\omega t}dt \quad (\alpha = x, y, z) \quad (3)$$

3. Results and discussion

At cryogenic temperatures, phonon thermal transport in non-metallic crystals is affected by a variety of special effects, including weakened phonon scattering and reduced heat capacity. From the perspective of numerical calculation of thermal conductivity, this specifically manifests as size effect and quantum effect. At cryogenic temperatures, the phonon energy in crystals is low, the structure is more stable, and the phonon-phonon interactions are relatively weak. Under the combined influence of these factors, phonons can propagate relatively undisturbed, indicating that they have longer MFP. However, in MD simulations, even when periodic boundary conditions are applied, systems with insufficient length can disrupt the phonon transport with long MFP, leading to an underestimation of thermal conductivity. Therefore, the assessment of the size effect is indispensable. Fig. 2(a) shows the size effect validation of thermal conductivity for the two models at 20 K, which include multiple sets with lengths ranging from approximately 30 nm to around 2.3 μm (about a million atoms). Thermal conductivity presented here is after the quantum correction, and details about it will be given later. This indicates that the thermal conductivity increases with increasing simulation size and starts to converge after the length exceeds 1 μm.

Based on HNEMD and its spectral heat current (SHC) decomposition method [38], Fig. S1 shows that at 20 K, the thermal conductivity calculated by classical MD is on the order of 10^4 $Wm^{-1}K^{-1}$. This significant overestimation is attributed to the oversight of the quantum effect in classical MD at low temperatures. Therefore, to obtain accurate and reasonable results, it is necessary to incorporate the quantum effect into consideration and engage in a detailed discussion.

For crystal materials such as graphene, diamond, and silicon with high thermal conductivity, the actual values of their thermal conductivity (experimental measurements) exhibit an unimodal trend of initially increasing and then decreasing with temperature. Near the low temperature limit, thermal conductivity essentially follows a cubic relationship with temperature, whereas at high temperatures, it exhibits an inverse relationship with temperature, as depicted in Fig. 2(b). However, the thermal conductivity calculated by MD simulation based on classical statistics exhibits a monotonically changing trend with temperature. At cryogenic temperatures, it exhibits a notable discrepancy, resulting in a significant overestimation of thermal conductivity. As the temperature rises to the intermediate range, typically in proximity to RT, the thermal conductivity in classical MD is slightly underestimated. This phenomenon can be attributed to the fact that classical MD not only overestimates the heat capacity, but also overestimates certain phonon-phonon scattering events, thus underestimating certain mean free paths [26]. At low temperatures, phonon scattering from defects, isotopes, and boundaries is dominant instead of phonon-phonon scattering. The interplay between these two effects is temperature-dependent: at cryogenic temperatures, the predominant overestimation is in heat capacity; as the temperature approaches RT, the overestimation of heat capacity becomes less pronounced, while the overestimation of phonon-phonon scattering takes precedence; and at high temperatures, classical MD provides a relatively accurate assessment of thermal conductivity.

More specifically, the phonon gas model indicates the heat capacity is a key indicator that determines the phonon thermal conductivity. In the energy equipartition theorem used by classical MD, the average energy of any degree of freedom of the equilibrium system is equal, and the modal heat capacity is a constant $C_c = k_B$, where k_B is the Boltzmann constant. In Bose-Einstein statistics that takes into account of quantum effects, the average number of phonons n at frequency ω is $n = (e^{\hbar\omega/k_BT} - 1)^{-1}$, where $\hbar$ is reduced Planck constant. The quantum modal heat capacity is $C_q = \hbar\omega \cdot \partial n/\partial T$. Defining $x = \hbar\omega/k_BT$, we have the quantum-to-classical ratio for heat capacity:

$$\alpha = \frac{C_q}{C_c} = \frac{x^2 e^x}{(e^x - 1)^2}, \quad (4)$$

as shown in Fig. 2(c) for selected temperatures. In the case of high temperature, i.e. $k_BT \gg \hbar\omega$, the harmonic oscillators are in highly excited states, with the energy of these states much greater than the quantum step. In this scenario, the quantum nature of the phonon vibrational spectrum becomes less significant, almost equivalent to the results described by classical theory. However, at low temperatures, i.e. $k_BT \ll \hbar\omega$, only those lattice waves with $\omega < k_BT/\hbar$ can be excited and therefore can contribute to the heat capacity. Lattice waves with frequencies higher than $k_BT/\hbar$ have been "frozen down" and do not contribute to the heat capacity. Furthermore, the mode-to-mode quantum correction results of SHC can be obtained by multiplying the SHC results of classical MD by the quantum correction factor α at the

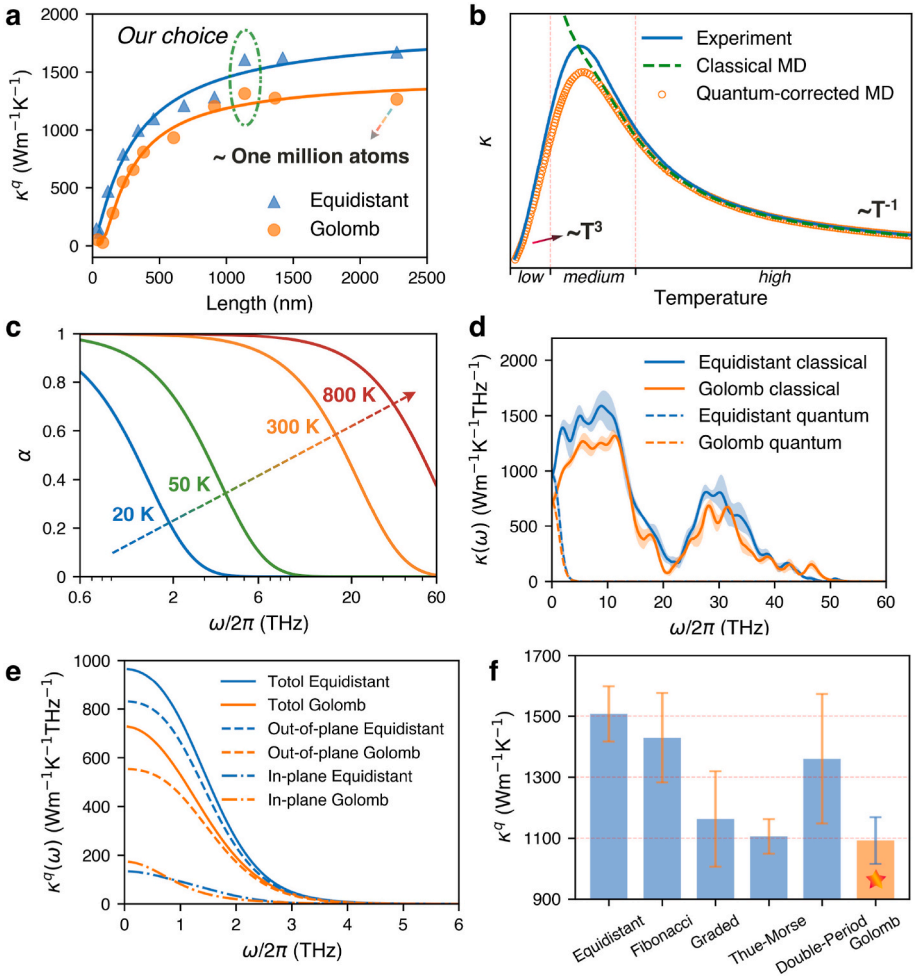

Fig. 2. Size effect and quantum effect of the thermal conductivity. (a) Quantum-corrected thermal conductivities change with system length at 20 K. (b) Schematic illustration of the relationship between thermal conductivity and temperature based on different methods. (c) Quantum correction coefficients at different temperatures. (d) Spectral thermal conductivity before and after quantum correction, where the shading is the standard error obtained from five independent simulations. (e) Quantum-corrected spectral thermal conductivity and its in-and-out-of-plane decomposition. (f) Comparison of thermal conductivity of graphene with different sequence isotopic interfaces at 20 K.

corresponding frequency. The effectiveness of this quantum correction method for current isotope doping systems stems from the fact that the phonon could be considered harmonic at cryogenic temperatures, and isotope scattering predominates instead of phonon-phonon scattering [26].

Fig. 2(d) illustrates the spectral thermal conductivity results of the Golomb ruler-based and equidistant interface structures at 20 K. The depiction includes the decomposition results of in-plane and out-of-plane contributions, along with a comparison before and after quantum correction. From the quantum-corrected spectral thermal conductivity in Fig. 2(e), the thermal conductivity of equidistant interface graphene (1508 ± 90 $Wm^{-1}K^{-1}$) is about 32 % higher than that of the Golomb ruler-based one (1092 ± 72 $Wm^{-1}K^{-1}$). And this gap is almost entirely due to out-of-plane low-frequency phonons. The detailed contribution percentage to thermal conductivity of different phonon frequencies are also characterized in Fig. S2.

Furthermore, based on other common mathematical sequences, including Fibonacci [45], Graded [46], Thue-Morse [47], and Double-Period [47] sequences, four graphene structures containing isotope interfaces were constructed, as shown in Fig. S3. Among them, Thue-Morse and Double-Period sequences are two types of quasi-periodic sequences, which are obtained from binary sequences through specific iterative inflation. During the model construction, due to the inherent differences in the sequences, it is impossible to guarantee that the interface density and isotope doping ratio between structures are exactly the same, but they should be made as close as possible to ensure good comparability among them. As shown in Fig. 2(f), at 20 K, the Golomb ruler-based interface structure has the lowest thermal conductivity, achieving the strongest suppression of phonon thermal transport.

In Fig. 3(a), the quantum-corrected thermal conductivity variations with the interface density are plotted for Golomb ruler-based and equidistant interface graphene at 20 K. Before proceeding further with the analysis of the data, we should clarify that all models with different interface densities have the same isotope doping ratio. Within the current range of interface density and considering the range of statistical errors, the thermal conductivity of both appears to be unaffected by changes in interface density. At such a cryogenic temperature, the phonon MFP is extremely large, making the aforementioned interface density changes insufficient to exert a substantial influence on phonon thermal transport.

The results at 300 K are depicted in Fig. 3(b) and are presented without quantum correction. As mentioned above, the overestimation of the heat capacity at RT by classical MD is not significant, and the correction may prove counterproductive. Chen et al. [30] measured the thermal conductivity of graphene with a ^{13}C doping ratio of 1.1 % by the micro-Raman spectrometer near RT and the result was 2600 ± 658 $Wm^{-1}K^{-1}$, which is in good agreement with our results. Fig. 3(b)

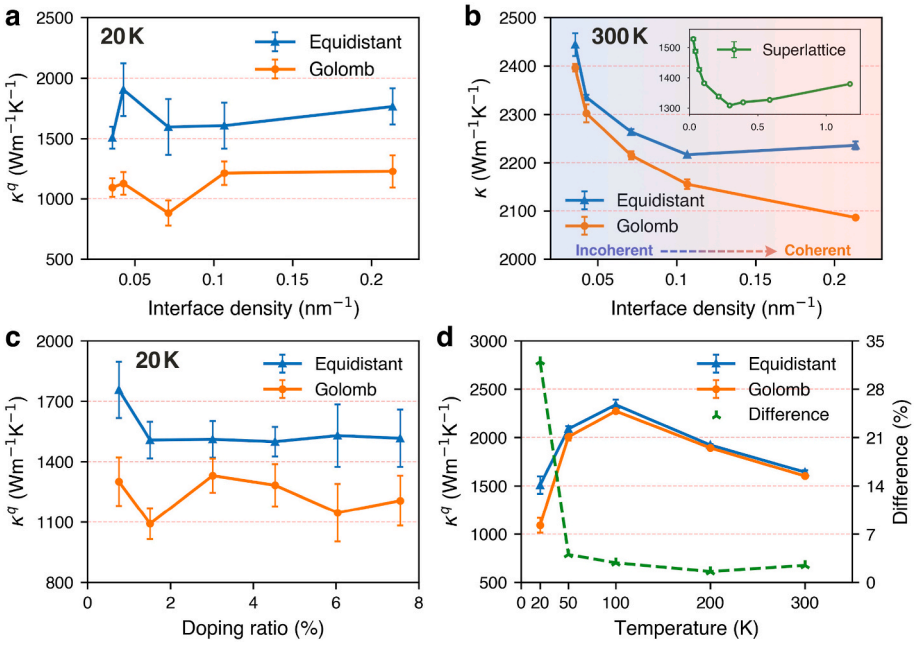

Fig. 3. Temperature effect and influence of structural parameters of equidistant and Golomb ruler structures. (a) Effect of interface density on their quantum-corrected thermal conductivities. (b) At room temperature, changes in interface density led to shifts in phonon transport coherence. And the subfigure is a result of the $^{12}C/^{13}C$ superlattice. (c) Effect of doping ratios on their quantum-corrected thermal conductivities. (d) Their quantum-correction thermal conductivities and differences at different temperatures.

indicates that with an increase in the interface density, the thermal conductivity of the equidistant interface structure exhibits an initial decrease followed by an increase. This trend aligns with the observed behavior of the phonon transport coherence transition in previous studies [48–50]. In contrast, the thermal conductivity of the Golomb ruler-based structure exhibits a consistently decreasing trend with increasing interface density. This implies that phonon transport no longer undergoes a transition from incoherence to coherence; instead, coherence disappears and the thermal conductivity consistently decreases with the increase of the interface density. In particular, when the isotope doping ratio reaches 50 %, the equidistant interface graphene turns into a $^{12}C/^{13}C$ lateral superlattice, as illustrated in Fig. S4. Results in Fig. 3(b) further indicate a distinct coherence transition feature in its phonon transport characteristics.

In addition, Fig. 3(c) illustrates the correlation between the isotope doping ratio and the thermal conductivity at 20 K. One should note that here the premise for discussing the doping rate is that the isotope interface exists and satisfies two sequence arrangements, which determine its lower limitation. It is also confined under 8 %, attributed to the constraints imposed by the minimum unit length of the Golomb ruler-based structure, as depicted in Fig. S4. Similar to the interface density, within the statistical margin of error, the doping ratio does not exert a significant influence on thermal conductivity. Fig. 3(d) plots the quantum corrected thermal conductivity and the difference between the Golomb ruler and the equidistant interface structure at different temperatures. The quantum-corrected thermal conductivity results from MD simulations here show a trend consistent with the experimental values as a function of temperature, as depicted in Fig. 2(b). Importantly, the significant gap between the two only exists under the cryogenic temperature of 20 K. Compared to other temperatures, at a cryogenic temperature of 20 K, the phonon energies are lower, and their energy levels become more dispersed, making it more sensitive to scattering caused by isotope interfaces. This temperature sensitivity offers flexibility for optimizing material properties in practical applications, providing significant implications for performance modulation across a broad temperature range.

To explore the cause of the difference above between the Golomb ruler-based interface graphene and the equidistant one, we performed additional phonon analyses. According to the phonon gas model, the phonon MFP denotes the average distance that phonons can traverse without scattering or encountering collisions as they propagate within a crystal structure. It is significant as it serves as a crucial indicator that influences the phonon thermal conductivity of a material. Fig. 4(a) illustrates the frequency-dependent phonon MFP for both the Golomb ruler-based interface structure and the equidistant one, along with their respective in-plane and out-of-plane contributions. Furthermore, Fig. S6 shows the results obtained by using the SHC method based on NEMD within the ballistic region.

The findings indicate a notable contrast in the phonon MFP between these two structures, particularly within the low-frequency regime, primarily spanning from 0 to 6 THz. Furthermore, the in-and-out-of-plane phonon contributions decomposition [51] reveals nearly identical in-plane phonon contributions for both structures. The observed distinction predominantly arises from the different contributions from out-of-plane phonons, which is also consistent with the results in Fig. 2 (d). In addition, Fig. 4(b) plots the size convergence of the quantum-corrected thermal conductivity of the two structures at 20 K, where the results are in good agreement with that of NEMD at the corresponding sizes. Due to the long phonon MFP at cryogenic temperatures, the thermal conductivity convergence is achieved near sub-millimeter lengths. The $\kappa(L)$ on the vertical axis represents the thermal conductivity of a finite-length system, as derived from the NEMD method. It should be noted that it is not directly comparable to the length obtained from the HNEMD method as depicted in Fig. 2(a) since the latter one is under the periodic boundary condition.

The phonon participation ratio (PPR) results in Fig. 4(c) show that no phonon localization at the low-frequency part which dominates thermal transport in these two systems. Furthermore, the phonon dispersion for both structures was calculated to analyze the influence of interfaces at different positions on the phonon scattering process, as depicted in Fig. 4 (d). The phonon dispersion curves show a dense distribution with a generally similar overall shape. However, distinctions are observed in their optical phonon branches. In comparison to the equidistant interface structure, the optical phonon branch of the Golomb ruler-based one

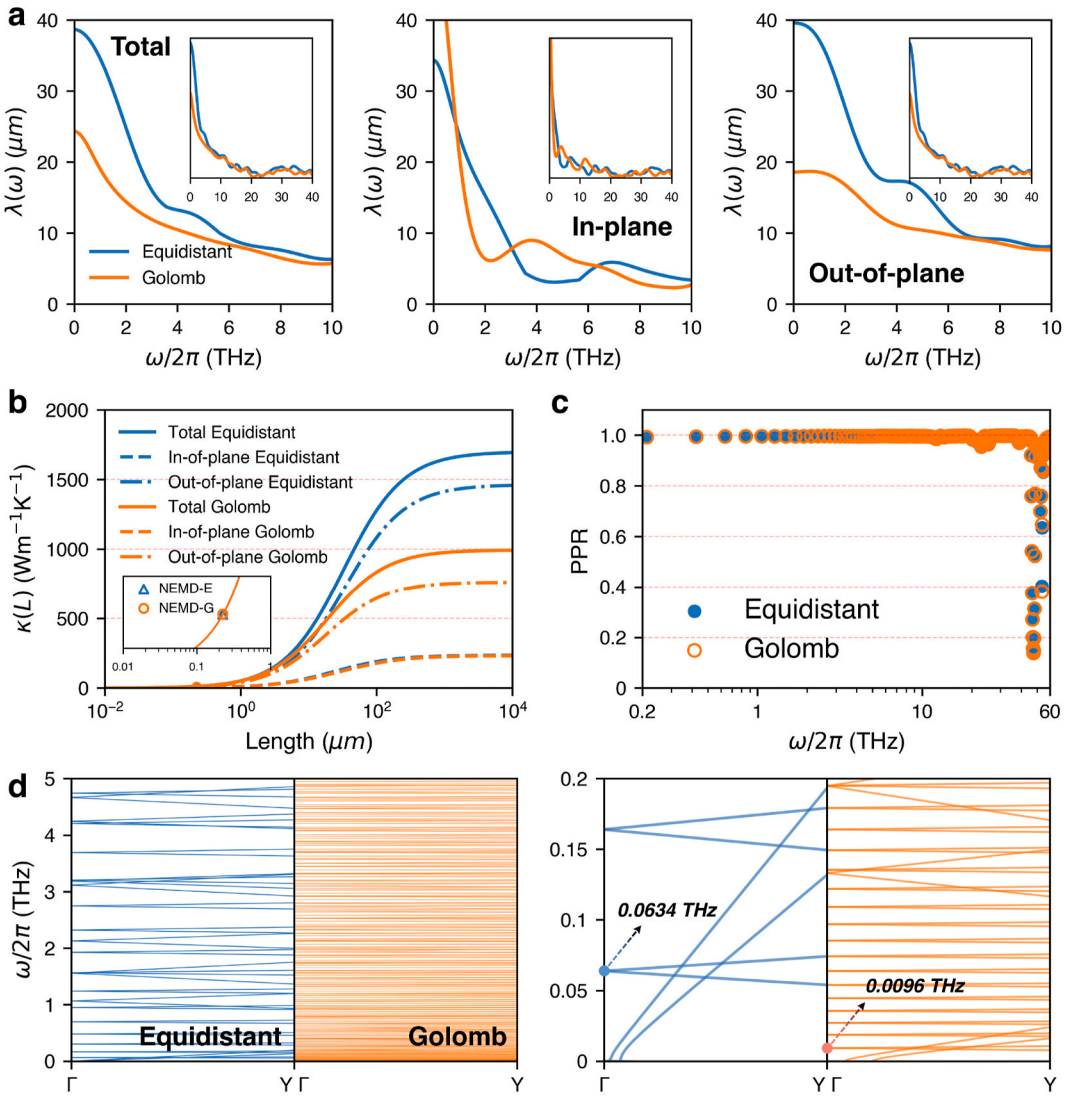

Fig. 4. Phonon analysis of the thermal conductivity difference between equidistant and Golomb ruler structures. (a) Spectral phonon mean free path and their in-and-out-of-plane decomposition. (b) Quantum-corrected thermal conductivity and their in-and-out-of-plane decomposition results as a function of length along the transport direction. (c) Phonon participation ratio versus phonon frequency. (d) Phonon dispersion curves for them. The one on the right is an enlarged display of the low-frequency band on the left.

experiences a downward shift. This shift implies the activation of numerous new scattering channels at lower frequencies, such as the merging of two acoustic phonons into one optical phonon through a three-phonon absorption process [52]. Consequently, the lower-frequency optical phonon branch intensifies the scattering of acoustic phonons in the Golomb ruler interface structure, thereby impeding its phonon thermal transport.

To obtain more phonon mechanism and visually discern the disparities in phonon transport between the two structures, we performed phonon wave packet simulations and subsequently presented the energy evolution results in Fig. 5. Specifically, we generated Gaussian phonon wave packets following space-dependent atomic displacement and

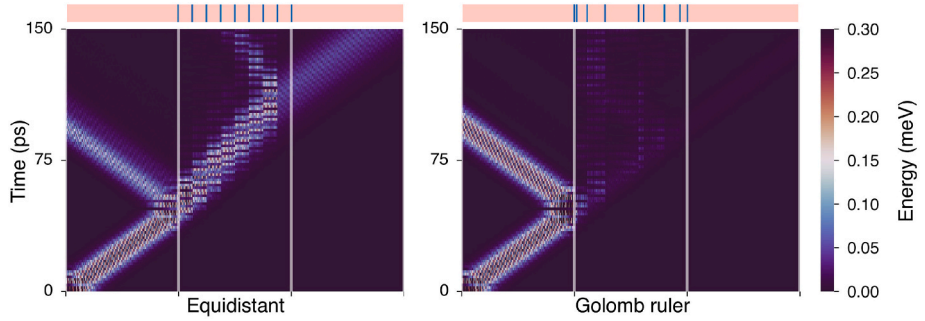

Fig. 5. Heatmap of the evolution of the wave-packet kinetic energies during the simulation time along the equidistant and Golomb ruler structures respectively.

monitored their propagation trajectories [24,53]:

$$u_{il\mu} = A_0 \epsilon_{i\mu\lambda}(k_0) e^{ik_0(x-x_0)} e^{-(x-x_0)^2/\eta^2}, \quad (5)$$

where A_0 represents the amplitude of the wave packet, $\epsilon_{i\mu\lambda}(k_0)$ is the polarization vector of the λ branch under the wave vector k_0, x_0 represents the center position and η is a parameter controlling the spatial extension of the wave packet. One should note that all wave packet simulations were performed at temperatures closely approaching 0 K, ensuring the system is as free from anharmonic states as possible.

Initially, a ZA wave packet is excited in the graphene functional region at the left end, and its progression into the target area is observed. Upon reaching the equidistant interface structure, a fraction of the wave packet is reflected, while the majority of which traverses through the target area, persisting in its onward trajectory. In contrast, when the same wave packet encounters the Golomb ruler-based interface structure, a significant portion undergoes reflection, and only a minimal fraction of the wave packets enter the target area. Moreover, the wave packets entering the target area are also confined within it, rendering them incapable of effective transmission. This reveals the pronounced obstructive effect of the Golomb ruler sequence interface on wave packets, and, consequently, phonon thermal transport.

4. Conclusions and outlook

In this work, through MD simulations with spectrum decomposition-based quantum correction, we investigated the impact of isotope interface position on phonon thermal transport in graphene nanoribbons. At a cryogenic temperature of 20 K, Golomb ruler-based isotope interfaces were found to significantly suppress thermal transport compared to equidistant ones. Moreover, a notable difference was observed only at extremely cryogenic temperatures because the effect may not manifest itself at higher phonon energies. Phonon analysis and wave packet simulations revealed that stronger coherent phonon scattering and confinement effects are fundamental reasons for the reduction in thermal conductivity of graphene with Golomb ruler isotope interfaces. This is also manifested in the significant decrease in the MFP of low-frequency out-of-plane phonons.

Future work, built on the theoretical foundations established in this study, will incorporate experimental studies to further strengthen understanding, which aligns with our ongoing research efforts. For sample preparation, the innovative work by Whiteway et al. [34], which utilized chemical vapor deposition (CVD) method to synthesize isotopic lateral heterostructures, will serve as a significant source of inspiration. And the time-domain thermoreflectance (TDTR) method would be a promising choice for measuring the thermal conductivity of this system [17]. In short, with graphene as the carrier, our theoretical exploration of the Golomb ruler sequence revealed significant thermal transport suppression, which has enlightening implications for the future design of systems with structural disordering across different fields.

CRediT authorship contribution statement

Xin Wu: Writing – review & editing, Writing – original draft, Visualization, Validation, Software, Methodology, Investigation, Formal analysis, Data curation, Conceptualization. **Yunhui Wu:** Writing – review & editing, Writing – original draft, Investigation, Data curation. **Xin Huang:** Writing – review & editing, Writing – original draft, Methodology, Investigation, Formal analysis. **Zheyong Fan:** Writing – review & editing, Writing – original draft, Software, Methodology, Formal analysis. **Sebastian Volz:** Writing – review & editing, Writing – original draft, Methodology. **Qiang Han:** Writing – review & editing, Writing – original draft, Project administration, Funding acquisition. **Masahiro Nomura:** Writing – review & editing, Writing – original draft, Supervision, Resources, Project administration, Investigation, Funding acquisition, Conceptualization.

Declaration of competing interest

The authors declare that they have no known competing financial interests or personal relationships that could have appeared to influence the work reported in this paper.

Data availability

Data will be made available on request.

Acknowledgments

This work was supported by the JSPS Grants-in-Aid for Scientific Research (Grant Nos. 21H04635 and 20H05649) and JST SICORP EIG CONCERT-Japan (Grant No. JPMJSC22C6). X. W. is the JSPS Post-doctoral Fellow for Research in Japan (No. P24058), and thanks the China Scholarship Council (CSC) for financial support (No. 202206150098). The authors are also grateful for support from the National Natural Science Foundation of China (11972160), Guangdong Basic and Applied Basic Research Foundation (2019A1515011900), Science and Technology Program of Guangzhou, China (202002030367).

Appendix A. Supplementary data

Supplementary data to this article can be found online at https://doi.org/10.1016/j.mtphys.2024.101500.

References

[1] F. Arute, K. Arya, R. Babbush, D. Bacon, J.C. Bardin, R. Barends, R. Biswas, S. Boixo, F.G.S.L. Brandao, D.A. Buell, B. Burkett, Y. Chen, Z. Chen, B. Chiaro, R. Collins, W. Courtney, A. Dunsworth, E. Farhi, B. Foxen, A. Fowler, C. Gidney, M. Giustina, R. Graff, K. Guerin, S. Habegger, M.P. Harrigan, M.J. Hartmann, A. Ho, M. Hoffmann, T. Huang, T.S. Humble, S.V. Isakov, E. Jeffrey, Z. Jiang, D. Kafri, K. Kechedzhi, J. Kelly, P.V. Klimov, S. Knysh, A. Korotkov, F. Kostritsa, D. Landhuis, M. Lindmark, E. Lucero, D. Lyakh, S. Mandrà, J.R. McClean, M. McEwen, A. Megrant, X. Mi, K. Michielsen, M. Mohseni, J. Mutus, O. Naaman, M. Neeley, C. Neill, M.Y. Niu, E. Ostby, A. Petukhov, J.C. Platt, C. Quintana, E. G. Rieffel, P. Roushan, N.C. Rubin, D. Sank, K.J. Satzinger, V. Smelyanskiy, K. J. Sung, M.D. Trevithick, A. Vainsencher, B. Villalonga, T. White, Z.J. Yao, P. Yeh, A. Zalcman, H. Neven, J.M. Martinis, Quantum supremacy using a programmable superconducting processor, Nature 574 (7779) (2019) 505–510, https://doi.org/10.1038/s41586-019-1666-5.

[2] R. Kato, M. Naya, N. Kasahata, R. Senga, C. Sato, M. Koshino, K. Suenaga, M. Hasegawa, Thermal management function of graphene under cryogenic temperature, Carbon 183 (2021) 970–976, https://doi.org/10.1016/j.carbon.2021.07.077.

[3] T. Chang, G. Zhao, Ice inhibition for cryopreservation: materials, strategies, and challenges, Adv. Sci. 8 (6) (2021): 2002425, https://doi.org/10.1002/advs.202002425.

[4] Z.E. Nataj, Y. Xu, D. Wright, J.O. Brown, J. Garg, X. Chen, F. Kargar, A.A. Balandin, Cryogenic characteristics of graphene composites—evolution from thermal conductors to thermal insulators, Nat. Commun. 14 (1) (2023) 3190, https://doi.org/10.1038/s41467-023-38508-3.

[5] D. van Delft, P. Kes, The discovery of superconductivity, Phys. Today 63 (9) (2010) 38–43, https://doi.org/10.1063/1.3490499.

[6] K.S. Novoselov, A.K. Geim, S.V. Morozov, D. Jiang, Y. Zhang, S.V. Dubonos, I. V. Grigorieva, A.A. Firsov, Electric field effect in atomically thin carbon films, Science 306 (5696) (2004) 666–669, https://doi.org/10.1126/science.1102896.

[7] A.K. Geim, K.S. Novoselov, The rise of graphene, Nat. Mater. 6 (3) (2007) 183–191, https://doi.org/10.1038/nmat1849.

[8] A. Gupta, T. Sakthivel, S. Seal, Recent development in 2D materials beyond graphene, Prog. Mater. Sci. 73 (2015) 44–126, https://doi.org/10.1016/j.pmatsci.2015.02.002.

[9] M.C. Lemme, D. Akinwande, C. Huyghebaert, C. Stampfer, 2D materials for future heterogeneous electronics, Nat. Commun. 13 (1) (2022) 1392, https://doi.org/10.1038/s41467-022-29001-4.

[10] A.K. Katiyar, A.T. Hoang, D. Xu, J. Hong, B.J. Kim, S. Ji, J.-H. Ahn, 2D materials in flexible electronics: recent advances and future prospectives, Chem. Rev. 124 (2) (2024) 318–419, https://doi.org/10.1021/acs.chemrev.3c00302.

[11] Q.-Y. Li, Q. Hao, T. Zhu, M. Zebarjadi, K. Takahashi, Nanostructured and heterostructured 2D materials for thermoelectrics, Engineered Science 13 (2021) 24–50, https://doi.org/10.30919/es8d1136.

[12] R. Yanagisawa, N. Tsujii, T. Mori, P. Ruther, O. Paul, M. Nomura, Nanostructured planar-type uni-leg Si thermoelectric generators, APEX 13 (9) (2020): 095001, https://doi.org/10.35848/1882-0786/aba5c4.

[13] H. Song, J. Liu, B. Liu, J. Wu, H.-M. Cheng, F. Kang, Two-dimensional materials for thermal management applications, Joule 2 (3) (2018) 442–463, https://doi.org/10.1016/j.joule.2018.01.006.
[14] H. Ma, E. O'Donnel, Z. Tian, Tunable thermal conductivity of π-conjugated two-dimensional polymers, Nanoscale 10 (2018) 13924–13929, https://doi.org/10.1039/C8NR02994F.
[15] S. Varghese, S. Varghese, S. Swaminathan, K. Singh, V. Mittal, Two-dimensional materials for sensing: graphene and beyond, Electronics 4 (3) (2015) 651–687, https://doi.org/10.3390/electronics4030651.
[16] C. Anichini, W. Czepa, D. Pakulski, A. Aliprandi, A. Ciesielski, P. Samorì, Chemical sensing with 2D materials, Chem. Soc. Rev. 47 (13) (2018) 4860–4908, https://doi.org/10.1039/C8CS00417J.
[17] X. Huang, Y. Guo, Y. Wu, S. Masubuchi, K. Watanabe, T. Taniguchi, Z. Zhang, S. Volz, T. Machida, M. Nomura, Observation of phonon Poiseuille flow in isotopically purified graphite ribbons, Nat. Commun. 14 (1) (2023) 2044, https://doi.org/10.1038/s41467-023-37380-5.
[18] Y. Machida, A. Subedi, K. Akiba, A. Miyake, M. Tokunaga, Y. Akahama, K. Izawa, K. Behnia, Observation of Poiseuille flow of phonons in black phosphorus, Sci. Adv. 4 (6) (2018): eaat3374, https://doi.org/10.1126/sciadv.aat3374.
[19] S. Lee, D. Broido, K. Esfarjani, G. Chen, Hydrodynamic phonon transport in suspended graphene, Nat. Commun. 6 (1) (2015) 6290, https://doi.org/10.1038/ncomms7290.
[20] G. Zhang, Y.-W. Zhang, Strain effects on thermoelectric properties of two-dimensional materials, Mech. Mater. 91 (2015) 382–398, https://doi.org/10.1016/j.mechmat.2015.03.009.
[21] L. Yang, Q. Zhang, G. Hu, N. Yang, Deformation insensitive thermal conductance of the designed Si metamaterial, Appl. Phys. Lett. 123 (2023): 062201, https://doi.org/10.1063/5.0158794.
[22] Y. Zhang, Q. Lv, H. Wang, S. Zhao, Q. Xiong, R. Lv, X. Zhang, Simultaneous electrical and thermal rectification in a monolayer lateral heterojunction, Science 378 (6616) (2022) 169–175, https://doi.org/10.1126/science.abq0883.
[23] Q.D. Gibson, T. Zhao, L.M. Daniels, H.C. Walker, R. Daou, S. Hébert, M. Zanella, M. S. Dyer, J.B. Claridge, B. Slater, M.W. Gaultois, F. Corà, J. Alaria, M.J. Rosseinsky, Low thermal conductivity in a modular inorganic material with bonding anisotropy and mismatch, Science 373 (2021) 1017–1022, https://doi.org/10.1126/science.abh161.
[24] S. Hu, Z. Zhang, P. Jiang, J. Chen, S. Volz, M. Nomura, B. Li, Randomness-induced phonon localization in graphene heat conduction, J. Phys. Chem. Lett. 9 (14) (2018) 3959–3968, https://doi.org/10.1021/acs.jpclett.8b01653.
[25] Z.-Y. Liu, J.-B. Pan, Y.-Y. Zhang, S.-X. Du, Beijing national laboratory for condensed matter physics, institute of physics, Chinese academy of sciences, Beijing 100190, China, university of Chinese academy of sciences, Beijing 100049, China, CAS center for excellence in topological quantum computation, Beijing 100190, China, songshan lake materials laboratory, dongguan 523808, China, first principles calculation of two-dimensional materials at an atomic scale, Acta Phys. Sin. 70 (2) (2021): 027301, https://doi.org/10.7498/aps.70.20201636.
[26] J.E. Turney, A.J.H. McGaughey, C.H. Amon, Assessing the applicability of quantum corrections to classical thermal conductivity predictions, Phys. Rev. B 79 (22) (2009): 224305, https://doi.org/10.1103/PhysRevB.79.224305.
[27] Y. Wang, Z. Fan, P. Qian, M.A. Caro, T. Ala-Nissila, Quantum-corrected thickness-dependent thermal conductivity in amorphous silicon predicted by machine learning molecular dynamics simulations, Phys. Rev. B 107 (5) (2023): 054303, https://doi.org/10.1103/PhysRevB.107.054303.
[28] S. Sidon, Ein satz über trigonometrische polynome und seine anwendung in der theorie der fourier-reihen, Math. Ann. 106 (1932) 536–539.
[29] W.C. Babcock, Intermodulation interference in radio systems, Bell System Technical Journal 32 (1) (1953) 63–73, https://doi.org/10.1002/j.1538-7305.1953.tb01422.x.
[30] S. Chen, Q. Wu, C. Mishra, J. Kang, H. Zhang, K. Cho, W. Cai, A.A. Balandin, R. S. Ruoff, Thermal conductivity of isotopically modified graphene, Nat. Mater. 11 (3) (2012) 203–207, https://doi.org/10.1038/nmat3207.
[31] Q.-X. Pei, Y.-W. Zhang, Z.-D. Sha, V.B. Shenoy, Carbon isotope doping induced interfacial thermal resistance and thermal rectification in graphene, Appl. Phys. Lett. 100 (10) (2012): 101901, https://doi.org/10.1063/1.3692173.
[32] J.-W. Jiang, J. Lan, J.-S. Wang, B. Li, Isotopic effects on the thermal conductivity of graphene nanoribbons: localization mechanism, J. Appl. Phys. 107 (5) (2010): 054314, https://doi.org/10.1063/1.3329541.
[33] Z. Tong, A. Pecchia, C. Yam, T. Dumitrică, T. Frauenheim, Phononic thermal transport along graphene grain boundaries: a hidden vulnerability, Adv. Sci. 8 (18) (2021): 2101624, https://doi.org/10.1002/advs.202101624.
[34] E. Whiteway, M. Lee, M. Hilke, Graphene isotope superlattices with strongly diminished thermal conductivity for thermoelectric applications, ACS Appl. Nano Mater. 3 (9) (2020) 9167–9173, https://doi.org/10.1021/acsanm.0c01802.
[35] M.E. Wieser, T.B. Coplen, Atomic weights of the elements 2009 (IUPAC technical report), Pure Appl. Chem. 83 (2) (2010) 359–396, https://doi.org/10.1351/PAC-REP-10-09-14.
[36] X. Wu, X. Huang, L. Yang, Z. Zhang, Y. Guo, S. Volz, Q. Han, M. Nomura, Suppressed thermal transport in mathematically inspired 2D heterosystems, Carbon 213 (2023): 118264, https://doi.org/10.1016/j.carbon.2023.118264.
[37] D.J. Evans, Homogeneous NEMD algorithm for thermal conductivity—application of non-canonical linear response theory, Phys. Lett. 91 (9) (1982) 457–460, https://doi.org/10.1016/0375-9601(82)90748-4.
[38] Z. Fan, H. Dong, A. Harju, T. Ala-Nissila, Homogeneous nonequilibrium molecular dynamics method for heat transport and spectral decomposition with many-body potentials, Phys. Rev. B 99 (6) (2019): 064308, https://doi.org/10.1103/PhysRevB.99.064308.
[39] Z. Li, S. Xiong, C. Sievers, Y. Hu, Z. Fan, N. Wei, H. Bao, S. Chen, D. Donadio, T. Ala-Nissila, Influence of thermostatting on nonequilibrium molecular dynamics simulations of heat conduction in solids, J. Chem. Phys. 151 (23) (2019): 234105, https://doi.org/10.1063/1.5132543, 10.1063/1.5132543.
[40] K. Sääskilahti, J. Oksanen, J. Tulkki, S. Volz, Role of anharmonic phonon scattering in the spectrally decomposed thermal conductance at planar interfaces, Phys. Rev. B 90 (13) (2014): 134312, https://doi.org/10.1103/PhysRevB.90.134312.
[41] K. Sääskilahti, J. Oksanen, S. Volz, J. Tulkki, Frequency-dependent phonon mean free path in carbon nanotubes from nonequilibrium molecular dynamics, Phys. Rev. B 91 (11) (2015): 115426, https://doi.org/10.1103/PhysRevB.91.115426.
[42] Z. Fan, W. Chen, V. Vierimaa, A. Harju, Efficient molecular dynamics simulations with many-body potentials on graphics processing units, Comput. Phys. Commun. 218 (2017) 10–16, https://doi.org/10.1016/j.cpc.2017.05.003. https://www.sciencedirect.com/science/article/pii/S0010465517301339.
[43] M.S. Green, Markoff random processes and the statistical mechanics of time-dependent phenomena. II. Irreversible processes in fluids, J. Chem. Phys. 22 (3) (1954) 398–413, https://doi.org/10.1063/1.1740082.
[44] R. Kubo, Statistical-mechanical theory of irreversible processes. I. General theory and simple applications to magnetic and conduction problems, J. Phys. Soc. Jpn. 12 (6) (1957) 570–586, https://doi.org/10.1143/JPSJ.12.570.
[45] I.M. Felix, L.F.C. Pereira, Suppression of coherent thermal transport in quasiperiodic graphene-hBN superlattice ribbons, Carbon 160 (2020) 335–341, https://doi.org/10.1016/j.carbon.2019.12.090.
[46] Y. Guo, M. Bescond, Z. Zhang, S. Xiong, K. Hirakawa, M. Nomura, S. Volz, Thermal conductivity minimum of graded superlattices due to phonon localization, Apl. Mater. 9 (9) (2021): 091104, https://doi.org/10.1063/5.0054921.
[47] I.M. Felix, L.F.C. Pereira, Thermal conductivity of thue–morse and Double-Period quasiperiodic graphene-hBN superlattices, Int. J. Heat Mass Tran. 186 (2022): 122464, https://doi.org/10.1016/j.ijheatmasstransfer.2021.122464.
[48] M.N. Luckyanova, J. Garg, K. Esfarjani, A. Jandl, M.T. Bulsara, A.J. Schmidt, A. J. Minnich, S. Chen, M.S. Dresselhaus, Z. Ren, E.A. Fitzgerald, G. Chen, Coherent phonon heat conduction in superlattices, Science 338 (6109) (2012) 936–939, https://doi.org/10.1126/science.1225549.
[49] M. Maldovan, Phonon wave interference and thermal bandgap materials, Nat. Mater. 14 (7) (2015) 667–674, https://doi.org/10.1038/nmat4308.
[50] J. Ravichandran, A.K. Yadav, R. Cheaito, P.B. Rossen, A. Soukiassian, S.J. Suresha, J.C. Duda, B.M. Foley, C.-H. Lee, Y. Zhu, A.W. Lichtenberger, J.E. Moore, D. A. Muller, D.G. Schlom, P.E. Hopkins, A. Majumdar, R. Ramesh, M.A. Zurbuchen, Crossover from incoherent to coherent phonon scattering in epitaxial oxide superlattices, Nat. Mater. 13 (2) (2014) 168–172, https://doi.org/10.1038/nmat3826.
[51] Z. Fan, L.F.C. Pereira, P. Hirvonen, M.M. Ervasti, K.R. Elder, D. Donadio, T. Ala-Nissila, A. Harju, Thermal conductivity decomposition in two-dimensional materials: application to graphene, Phys. Rev. B 95 (14) (2017): 144309, https://doi.org/10.1103/PhysRevB.95.144309.
[52] T. Liang, K. Xu, M. Han, Y. Yao, Z. Zhang, X. Zeng, J. Xu, J. Wu, Abnormally high thermal conductivity in fivefold twinned diamond nanowires, Materials Today Physics 25 (2022): 100705, https://doi.org/10.1016/j.mtphys.2022.100705.
[53] P.K. Schelling, S.R. Phillpot, P. Keblinski, Phonon wave-packet dynamics at semiconductor interfaces by molecular-dynamics simulation, Appl. Phys. Lett. 80 (14) (2002) 2484–2486, https://doi.org/10.1063/1.1465106.